Complete wavefront reconstruction using sequential intensity measurements of a volume speckle field

Percival Almoro, Giancarlo Pedrini, and Wolfgang Osten

The recording of the volume speckle field from an object at different planes combined with the wave propagation equation allows the reconstruction of the wavefront phase and amplitude without requiring a reference wave. The main advantage of this single-beam multiple-intensity reconstruction (SBMIR) technique is the simple experimental setup because no reference wave is required as in the case of holography. The phase retrieval technique is applied to the investigation of diffusely transmitting and reflecting objects. The effects of different parameters on the quality of reconstructions are investigated by simulation and experiment. Significant enhancements of the reconstructions are observed when the number of intensity measurements is 15 or more and the sequential measurement distance is 0.5 mm or larger. Performing two iterations during the reconstruction process using the calculated phase also leads to better reconstruction. The results from computer simulations confirm the experiments. Analysis of transverse and longitudinal intensity distributions of a volume speckle field for the SBMIR technique is presented. Enhancing the resolution method by shifting the camera a distance of a half-pixel in the lateral direction improves the sampling of speckle patterns and leads to better quality reconstructions. This allows the possibility of recording wave fields from larger test objects.

OCIS codes: 100.5070, 100.3010, 030.6140, 030.1640, 050.1960, 090.0090.

1. Introduction

Complete wavefront reconstruction with both amplitude and phase information is a vital part in many technical and scientific applications. The various ways by which a wavefront may be reconstructed can be placed in two groups: (1) methods with a reference beam (interferometry) and (2) methods without a reference beam (phase retrieval). Reconstruction methods with some forms of reference beamlike holography and speckle interferometry have been extensively utilized in 3D imaging and in nondestructive testing.[1,2] Configuring a separate reference beam from a single laser source, however, entails additional optical components and reduces the available laser power. Furthermore, configuring and recording the interference pattern formed by the superposition of the information-carrying beam and the reference beam involve a tedious and sometimes cumbersome process of optimizing the beam ratio and fringe spacing. Reconstruction methods without a reference beam or those commonly referred to as phase retrieval methods have been utilized in the optical microscopy of phase objects[3] and in the imaging of nanoparticles using electron microdiffraction patterns.[4] Phase retrieval methods utilize the change in two intensity measurements of a wave field to reconstruct the phase of an object wave. Depending on the methods used, various constraints and approximations are required and some constraints are to be given as *a priori* knowledge. Iterative phase retrieval methods such as those based on Gerchberg–Saxton (GS) and Yang–Gu (YG) algorithms, for example, are subject to a constraint that the test object is known to be either a phase-only or an amplitude-only object.[5–7] Deterministic phase retrieval methods such as those based on the intensity-transport and phase-transport equations assume a paraxial approximation or that light propagates strictly in one direction.[8–10] When applied to the general case for speckle fields, which do not propagate strictly in one direction, the validity of using these methods is limited.[10] Phase retrieval methods have also been utilized to reconstruct in-line digital holograms to eliminate the twin-image problem.[11–13] Since in-line holography means that a large portion of

All the authors are with the Institut für Technische Optik, Universität Stuttgart, Pfaffenwaldring 9, Stuttgart 70569, Germany. P. Almoro (almoro@ito.uni-stuttgart.de) is on leave from the National Institute of Physics, University of the Philippines, Diliman, Quezon City 1101, Philippines.

Received 30 May 2006; accepted 2 August 2006; posted 11 August 2006 (Doc. ID 71495).

0003-6935/06/348596-10$15.00/0

the wave illuminating the object scene serves as the reference beam, recording is done in the transmission mode but not in the reflection mode and, hence, its range of applications is also limited.

Recently an alternative reconstruction method without a reference beam, the single-beam multiple-intensity reconstruction (SBMIR) technique using only the intensity measurements of a volume speckle field and wave propagation equation, has been demonstrated.[14] The SBMIR technique is a promising wavefront reconstruction method because it offers a simple setup and a straightforward procedure. Compared to other phase retrieval methods such as those based on the GS and YG algorithms, the SBMIR technique is applicable to amplitude and/or phase objects and in both transmission and reflection modes. Compared to phase retrieval methods based on intensity-transport and phase-transport equations, this technique, which fully utilizes the multiple intensity measurements of a volume speckle field, is especially adaptive to speckle fields that propagate in all directions.

In previous work, the SBMIR technique was demonstrated experimentally by using a transmission mask as the test object. It was shown by simulation that the reconstruction improves with more intensity measurements. In the present work, the SBMIR technique is demonstrated using diffusely transmitting and reflecting objects. The effects of the number of intensity measurements, iterations, and sequential measurement distance are investigated by simulations and experiments. The sampling of speckle patterns can be improved by enhanced resolution methods. It has been shown in digital holography that the quality of reconstructions and interferograms significantly increase by enhancing the resolution of the detection system using subpixel scanning in the recording of the holograms.[15] We will demonstrate better quality wavefront reconstructions using an enhanced resolution method and the SBMIR technique.

In Section 2, the experimental setup and general methods for the intensity measurements of a volume speckle field are discussed. The principles and equations for the reconstruction of wave fields using the SBMIR technique are presented in Section 3. The various investigations, specific methods used, and results are discussed in Section 4. Finally, the conclusions are summarized in Section 5.

2. Intensity Measurements of Volume Speckle Field

Figure 1 shows the experimental setup for the recording of a volume speckle field. When a coherent light such as a laser illuminates the rough surface of an object it generates a volume speckle field. This 3D speckle field is characterized by grainy and random intensity distribution arising from the interference between closely spaced and randomly phased scatterers within the microstructures of the object surface.[16] The intensities of the speckle patterns (I_1, I_2, . . . , I_N) at equal-interval planes are sequentially measured using a CCD camera (Teli B/W C3910, 1300 × 1030 pixels) and a frame grabber and stored in the computer. The CCD pixel size ($\Delta x \times \Delta y$) is 6.7 μm × 6.7 μm and the total sensing area has dimensions of 8.7 mm × 6.9 mm. Applying the Nyquist sampling condition along one direction, the smallest speckle size that can be recorded would be at least equal to two pixels ($2\Delta x$) or 13.4 μm. This means that, with a He–Ne laser with an output wavelength λ of 0.633 μm, a uniformly illuminated circular object 1 mm in diameter (D) should be positioned at least 20 mm from the CCD in order to satisfy the sampling condition (i.e., $z \geq 2\Delta x D/\lambda$). The camera is sequentially moved between the measurement planes with a distance of Δz using a motorized precision stage [Physik Instrumente (PI), resolution 0.01 μm, maximum velocity 1.5 mm/s]. The cycle of intensity measurement and camera stage movement is repeated over a certain number (N) of measurement planes. As an idea for the recording time for N cycles, 20 intensity measurements at 1 mm distance interval would take about 1 min. A faster recording time could still be achieved with better and more optimized control of the stage and detector system. From the sequentially measured intensities, the complete object wave field will be reconstructed.

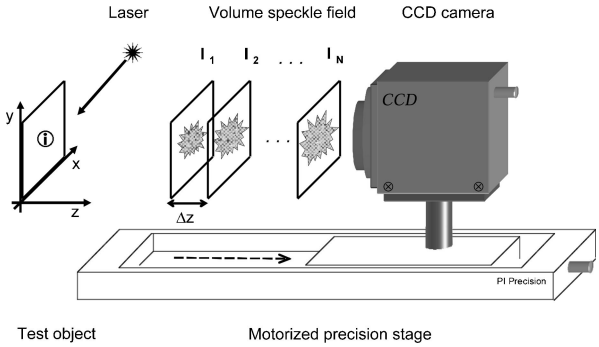

Fig. 1. Diagram for sequential intensity measurements of volume speckle field.

3. Reconstruction of Wave Fields

Figure 2 shows the diagram for the reconstruction of the test object wave field represented by intensity I_0 and phase ϕ_0 located at the origin. The measured intensities are utilized to reconstruct the object wave field. In the experiment, only 1024 × 1024 pixels of the originally measured intensities are used for expediency in the reconstruction algorithm. The reconstruction process starts with the wave amplitude being obtained from the square root of the first

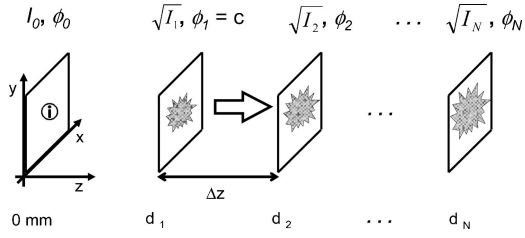

Fig. 2. Diagram for wave field reconstruction.

intensity distribution measured at position d_1. This amplitude is multiplied by the phase (initially a constant) and the resulting complex-valued function representing the wave field at that particular plane is propagated to the next plane. The propagation of the wave according to the Rayleigh–Sommerfeld equation is given by[16]

$$U(x, y, z) = u\int\int \hat{u}(f_x, f_y)\exp\left[(-i2\pi z/\lambda) \times (1-\lambda^2 f_x^2 - \lambda^2 f_y^2)^{1/2}\right]\exp[-i2\pi(f_x x + f_y y)] \times df_x df_y, \quad (1)$$

where U is the wave field at the output plane; $\hat{u}$ is the Fourier transform of the wave field at the input plane; the first exponential term in the integrand is the transfer function of free-space propagation; z is the propagation distance; and f_x and f_y are spatial frequencies in the x and y directions, respectively. By sampling the intensity distributions into the $m \times n$ matrix at each measurement plane and using the convolution theorem, Eq. (1) in numeric form is given by

$$\begin{aligned} U_{p+1}(k\Delta x', l\Delta y', z) &= A_{p+1}(k\Delta x', l\Delta y', z) \times \exp[i\varphi_{p+1}(k\Delta x', l\Delta y', z)] \\ &= \Im^{-1}\Bigg(\Im\{[I_p(m\Delta x, n\Delta y)]^{1/2} \times \exp[i\varphi_p(m\Delta x, n\Delta y)]\} \\ &\quad \times \exp\Bigg[(-i2\pi z/\lambda) \times \left(1 - \frac{\lambda^2 m^2}{\Delta x^2} - \frac{\lambda^2 n^2}{\Delta y^2}\right)^{1/2}\Bigg]\Bigg), \end{aligned} \quad (2)$$

where U_{p+1} is the complex amplitude calculated at the $(p+1)$ plane, $p = 1 \ldots (N-1)$; A_{p+1} and φ_{p+1} are the calculated amplitude and phase, respectively; $(k\Delta x', l\Delta y')$ and $(m\Delta x, n\Delta y)$ are the coordinates at the $(p+1)$ and p planes, respectively; $\Im$ denotes 2D Fourier transformation; I_p is the intensity distribution measured at the p plane; and $\Delta x \times \Delta y$ are the dimensions of the CCD pixels. For the next propagation, φ_{p+1} is retained while A_{p+1} is replaced by the square root of the intensity distribution measured at the $(p+1)$ plane. The new wave function at the $(p+1)$ plane, i.e., $(I_{p+1})^{1/2}\exp(i\varphi_{p+1})$, is then propagated to the $(p+2)$ plane. The process of multiplying the square root of the measured intensity distribution with the calculated phase at each plane followed by wave propagation is repeated until the quality of the reconstructed image at the object plane changes by amounts that are smaller than some threshold. Increasing the number of intensity measurements utilized for the SBMIR technique will result in a better approximation of the true phase. Intensity correlation may be used to quantify the similarity of the test object and the reconstructed wave intensity at the object plane. A threshold value for the correlation may be set for satisfactory wavefront reconstruction. The calculated wavefront in the measurement planes should also exhibit numerical focusing when propagated back to the image space.

4. Results and Discussion

A. Numerical Focusing

One indication of good phase reconstruction is when the calculated wave can be brought into focus at a given plane and this focused wave is comparable with a known object intensity distribution at that plane. In the foreground and background of this object plane the intensities of the propagated wave are expected to be defocused. Best-focused reconstruction can be gauged if the normalized correlation peak value with respect to a known focused image of the test object is a maximum. Perfect correlation (maximum correlation of 1) between the reconstructed intensity and the test object, however, can only be achieved with a very large CCD sensing area. Qualitative evaluation for an array of reconstructions at different planes may also complement the quantitative correlation process. In this study, correlations will be performed in the computer simulations only. For the computer simulations, the simulated rough object is a 1024×1024 pixel image of the ITO logo rendered with random intensity and phase distributions. The dimension of the whole logo is 300×300 pixels and the thickness of the elements of the logo is 20 pixels. These dimensions of the simulated object will correspond to the dimensions in the physical experiment. With the given CCD pixel size, the dimension of the whole logo is equal to 2.01×2.01 mm and the thickness of its elements is 134 μm. Figure 3(a) shows an array of five reconstructions from the simulations starting from the foreground planes (left) to the object plane (middle) and into the background planes (right) at 2 mm intervals. The focusing of the logo at the middle of the array evidently shows that wavefront reconstruction is achieved. In comparison, Fig. 3(b) shows the reconstructions at the same observation planes as in Fig. 3(a) but this time from a single intensity measurement multiplied by a constant phase. It is clear from Fig. 3(b) that, since no focusing happened, a single intensity measurement multiplied by a mere constant phase, which is far from the

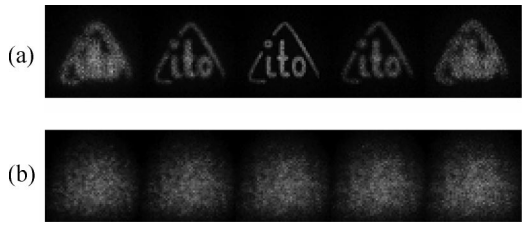

Fig. 3. (a) Array of reconstructions from multiple intensity measurements at 2 mm interval reconstruction planes. (b) Corresponding array of reconstructions from a single intensity measurement.

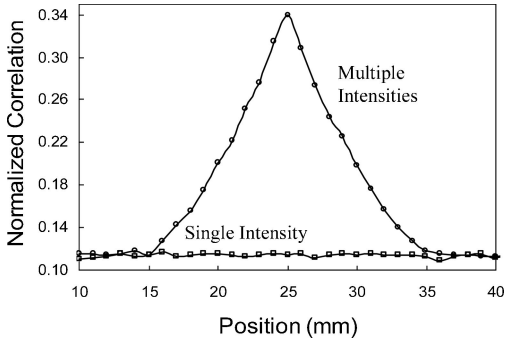

Fig. 4. Correlations of reconstructions at different positions for multiple intensity measurements and a single intensity measurement.

true phase, will not be sufficient to reconstruct the complete wave. Figure 4 shows a plot of the normalized correlation between the simulated object and the reconstructions as a function of position. At 25 mm the correlation peak for the case of multiple intensity reconstructions is at a maximum with a value of about 0.34. To the left and right of this position the plot shows decreasing values of correlation that indicate that the reconstructions become less similar to the simulated object. This is apparent from the defocusing of the reconstructed image in the foreground and background regions in Fig. 3(a). For the case of a single intensity measurement, the completely defocused reconstructions resulted in an almost constant low correlation value.

Figure 5 shows the experimental results for a diffusely transmitting object. The test object used is a transmitting mask with a ground glass diffuser attached to it to effect phase randomization. The width of the whole object is 2 mm and the thickness of the elements is about 200 μm. Figure 5(a) shows an array of five reconstructions at 2 mm interval planes obtained from using multiple intensity measurements. The similar focusing effect of the wave intensity at the object plane (middle of array) like that observed in the simulations confirms the wavefront reconstruction using the SBMIR technique. In contrast, Fig. 5(b) shows the corresponding array of nonfocusing reconstructions obtained from using a single intensity measurement. Figure 6 shows the experimental results for a diffusely reflecting object. The test object is a star with a white outline on a black background and printed on bond paper. The diameter

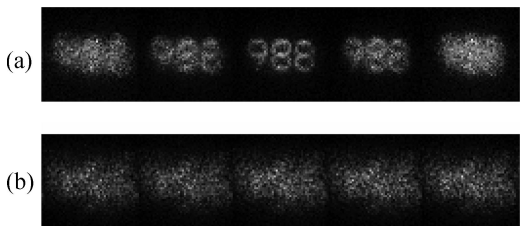

Fig. 5. Reconstructions of a diffusely transmitting object at 2 mm interval reconstruction planes using (a) multiple intensity measurements and (b) a single intensity measurement.

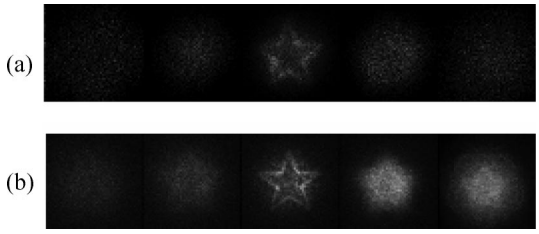

Fig. 6. (a) Reconstructions of a diffusely reflecting object at 2 mm interval reconstruction planes. (b) Photographic images obtained using a lens imaging system.

of the whole object is 3 mm and the thickness of the lines is about 250 μm. Figure 6(a) demonstrates focusing of the wave from a reflecting object using the SBMIR technique. For comparison, Fig. 6(b) shows an array of photographic images captured using a conventional lens imaging system. Note the presence of speckles even in the best focused image (middle), which is due to the coherent illumination light source used. Similar spatial characteristics are observed in the reconstructions in Fig. 6(a).

B. Effects of Number of Intensity Measurements

The optimum number of intensity measurements for satisfactory wavefront reconstruction may not be easy to ascertain because of the effects of various experimental factors and the extent of phase randomization occurring on particular object surfaces. Factors such as intensity saturations and background noise during measurements may introduce errors that are subsequently propagated in the process. The degree of roughness for different objects may introduce varying degrees of phase randomizations. In the measurements of intensities, this issue can be related to the finite size and limited resolution of detectors. The objective of this investigation is to approximate the number of intensity measurements that will result in good reconstructions using simulations and experiments. Performing iterations during the reconstruction process will also be investigated by multiplying the first intensity measurement for the next iteration using the calculated phase from the previous iteration. In principle, iteration should improve the reconstructions because the phase derived from the reconstruction process is more accurate than a mere constant phase being multiplied to the amplitude at the first recording plane. This may lead to a reduction of the number of intensities to be measured. Figure 7 shows a matrix of representative reconstructions from simulations to demonstrate the effects of the number of intensity measurements and number of iterations on the quality of reconstructions. Moving down a column, the number of intensity measurements used to reconstruct the wave is increased (reconstructions using 5, 10, 15, and 20 intensity measurements are shown). Moving from left to right the number of iterations is increased from 1 to 5. Note that the top two rows, the reconstructions using 5 and 10 measurements only, do not result in acceptable image quality even after 5 iterations. The

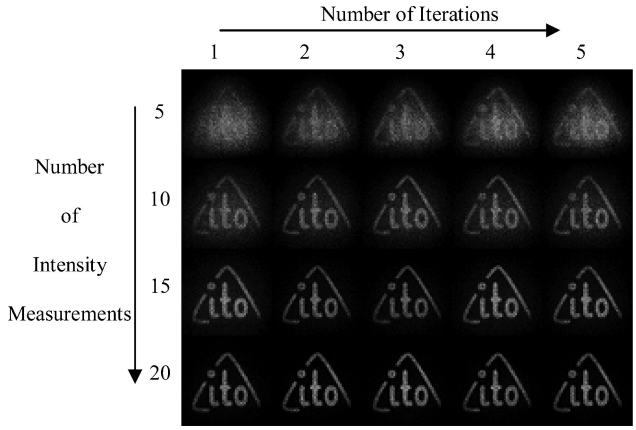

Fig. 7. Simulations of the effects of number of intensity measurements and iterations on the quality of reconstructions.

aspects of the logo are not sharp and the intensity distributions are generally noisy. Also perceptible in a close-up of the first column (1 iteration) is the significant improvement of image quality after 20 measurements. For the second through fifth columns (2, 3, 4, and 5 iterations) significant improvements started after 15 measurements only. For a more accurate evaluation of image quality the reconstructions are correlated with the simulated object. Figure 8 shows the plots of normalized correlations as a function of the number of intensity measurements and number of iterations. The curves are positively sloped and taper off after about 15 to 20 measurements. The positive slopes indicate an increase in image quality with an increasing number of intensity measurements. Also evident is the grouping of the curves corresponding to 2, 3, 4, and 5 iterations. This means that at least two iterations (solid curve with circles) will already result in significant improvements and further iterations may only entail longer processing time. Based on the qualities of the reconstructions in this simulation a correlation threshold of 0.3 may be set for satisfactory reconstructions. This threshold value signifies that 20 intensity measurements and at least two iterations may be sufficient to obtain satisfactory wavefront reconstruction.

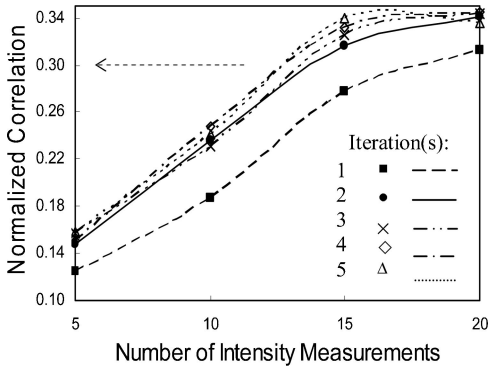

Fig. 8. Correlations of reconstructions for an increasing number of intensity measurements and iterations.

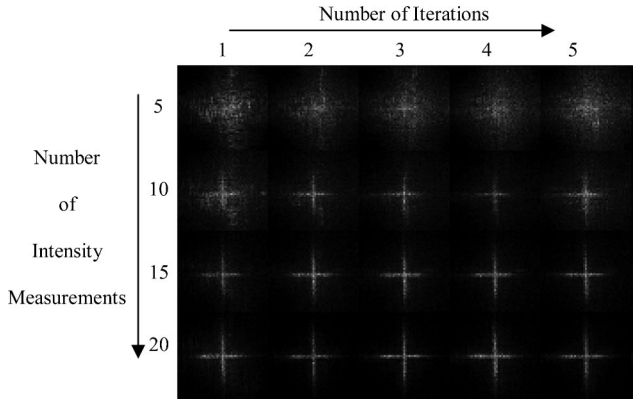

Fig. 9. Reconstructions of a diffusely transmitting object for increasing number of intensity measurement and iterations.

For the experiments the test object used is a transmission mask with a ground glass diffuser. The element in the test object is a cross hair (or a plus sign) with dimensions of 2 mm and a thickness of about 200 μm. Figure 9 shows a matrix of reconstructions for increasing the number of intensity measurements (5, 10, 15, and 20) and for one to five iterations. Again noticeable is the poor quality of reconstructions in the top two rows corresponding to 5 and 10 measurements. In the first column (single iteration) noise is still apparent even after 20 measurements. In comparison, in the second column (two iterations) the reconstruction after 20 measurements is evidently improved. As a further note, when the SBMIR technique is implemented in the opposite direction by proceeding from the Nth measurement plane to the first measurement plane, similar results for the reconstructions are obtained.

To establish the fact that using only two speckle intensity measurements would not be sufficient to reconstruct the wavefront from a rough object despite a large number of iterations, simulation and experiment were conducted. Two measurement distances were considered: a small distance of $\Delta z = 0.5$ mm and a large distance of $\Delta z = 1.0$ mm. Figure 10 shows a matrix of representative nonreconstructions at the object plane obtained using two intensity measurements for increasing the number of iterations from 100, 200, . . . , 500. The first and second rows show nonreconstructions obtained from simulations when only two speckle intensity measurements are used. Results from experiments (third and fourth rows) also demonstrate similar nonreconstructions. For comparison, reconstructions obtained using 20 intensity measurements, $\Delta z = 0.5$ mm, and two iterations are shown on the right-hand side of Fig. 10. The results shown here emphasize the importance of using multiple intensity measurements of a volume speckle field in reconstructing the object wavefront.

C. Effects of Sequential Measurement Distance

The distance between sequential measurement planes also affects the quality of reconstruction because the improvement of the phase depends on the variation of

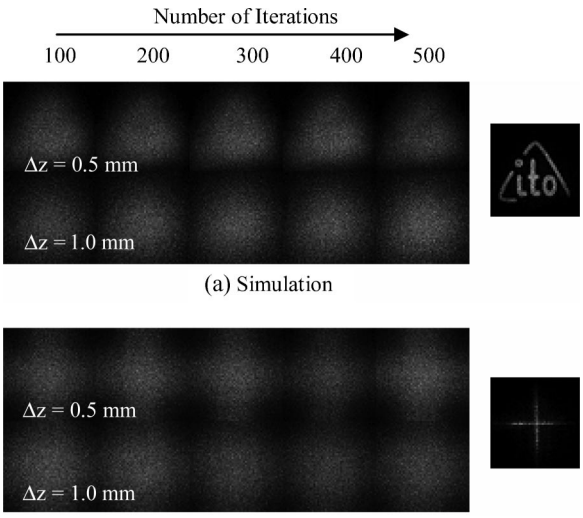

Fig. 10. Nonreconstructions obtained from two intensity measurements separated by 0.5 and 1.0 mm, despite the large number of iterations. For comparison, the images at right show good reconstructions when multiple intensity measurements are used.

intensity that, in turn, depends on the distance. If the distance is very small, the intensity distributions do not change substantially. The objective of this investigation is to determine the minimum sequential measurement distance that will result in satisfactory reconstructions. Figure 11 shows an array of reconstructions, from left to right, corresponding to specific cases when the measurement distances are $\Delta z = 0.1$ mm, $\Delta z = 0.2$ mm, . . . , $\Delta z = 1$ mm, for the same number of intensity measurements ($N = 20$). It is observed that significant improvements started with 0.3 or 0.4 mm measurement distances. For a quantitative analysis, Fig. 12 shows the plot of the correlation as a function of measurement distance. Setting a correlation threshold value of 0.3, a measurement distance of 0.5 mm may be considered the minimum distance to achieve satisfactory reconstructions for this particular object wavefront. A similar observation on the effect of measurement distance was noted when the speckle volume being sampled is kept constant (for a volume depth $N\Delta z = 20$ mm) with a varying number of intensity measurements. Figure 13 shows the experimental results using a diffusely transmitting mask where poor reconstructions are also evident in the cases of small measurement distances, especially for $\Delta z = 0.1$ mm (leftmost). Qualitatively, for this particular object used, the reconstruction from 0.5 mm measurement distance may be considered a good quality reconstruction. This value for the measurement distance is about the same value

Fig. 11. Simulations of the effects of increasing sequential measurement distance (from left to right): $\Delta z = 0.1$ mm, $\Delta z = 0.2$ mm, . . . , $\Delta z = 1$ mm.

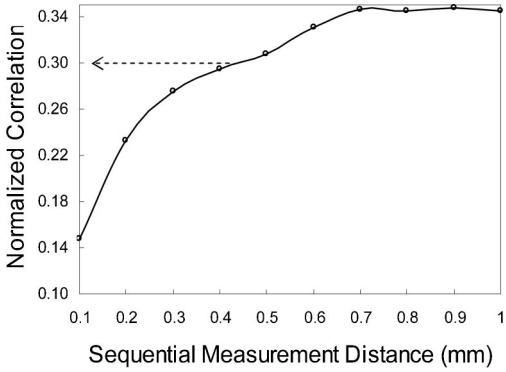

Fig. 12. Correlation as a function of measurement distance (Δz).

observed in the simulations. In addition, if the measurement distance is very large ($\Delta z > 10$ mm), poor reconstructions were obtained that may be attributed to the limited detector sensing area.

D. Analysis of Volume Speckle Field

In this subsection the intensity and phase distributions of a volume speckle field are investigated in order to derive some insights on the reconstruction process taking place using the SBMIR technique. Phase reconstruction using the SBMIR technique greatly depends on the quality of the sequential intensity measurements of the volume speckle field. Efficient sampling of the speckle patterns and variation in the intensity distributions measured at adjacent planes are essential for enhanced wavefront reconstruction. Figure 14(a) shows the schematic of a volume speckle field and indicates the observation planes of interest: A, B, and C. The test object used is a white circular dot (1 mm in diameter) on a black background and printed on bond paper. Upon illumination by a coherent beam from a He–Ne laser ($\lambda = 633$ nm), the scattered light generates the volume speckle field. The sequential intensity measurements are taken in the region starting from $d_1 = 40$ mm up to $d_N = 60$ mm from the test object. Within a volume depth of 20 mm, 200 intensity measurements are taken at a measurement distance of 100 μm.

The transverse intensity and phase distributions of the volume speckle field will be examined in relation to detector sampling and intensity saturation. In plane A (first measurement plane) the mean speckle size must satisfy the sampling condition and the speckle intensity levels must not be saturated. In plane B (Nth measurement plane) the intensity levels of the speckle bright spots must be sufficient for detector sensitivity. Figures 14(b) and 14(c) are zoomed-in sections of the intensity measurements in

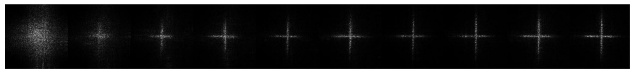

Fig. 13. Reconstructions for a diffusely transmitting object for increasing measurement distance (from left to right): $\Delta z = 0.1$ mm, $\Delta z = 0.2$ mm, . . . , $\Delta z = 1$ mm.

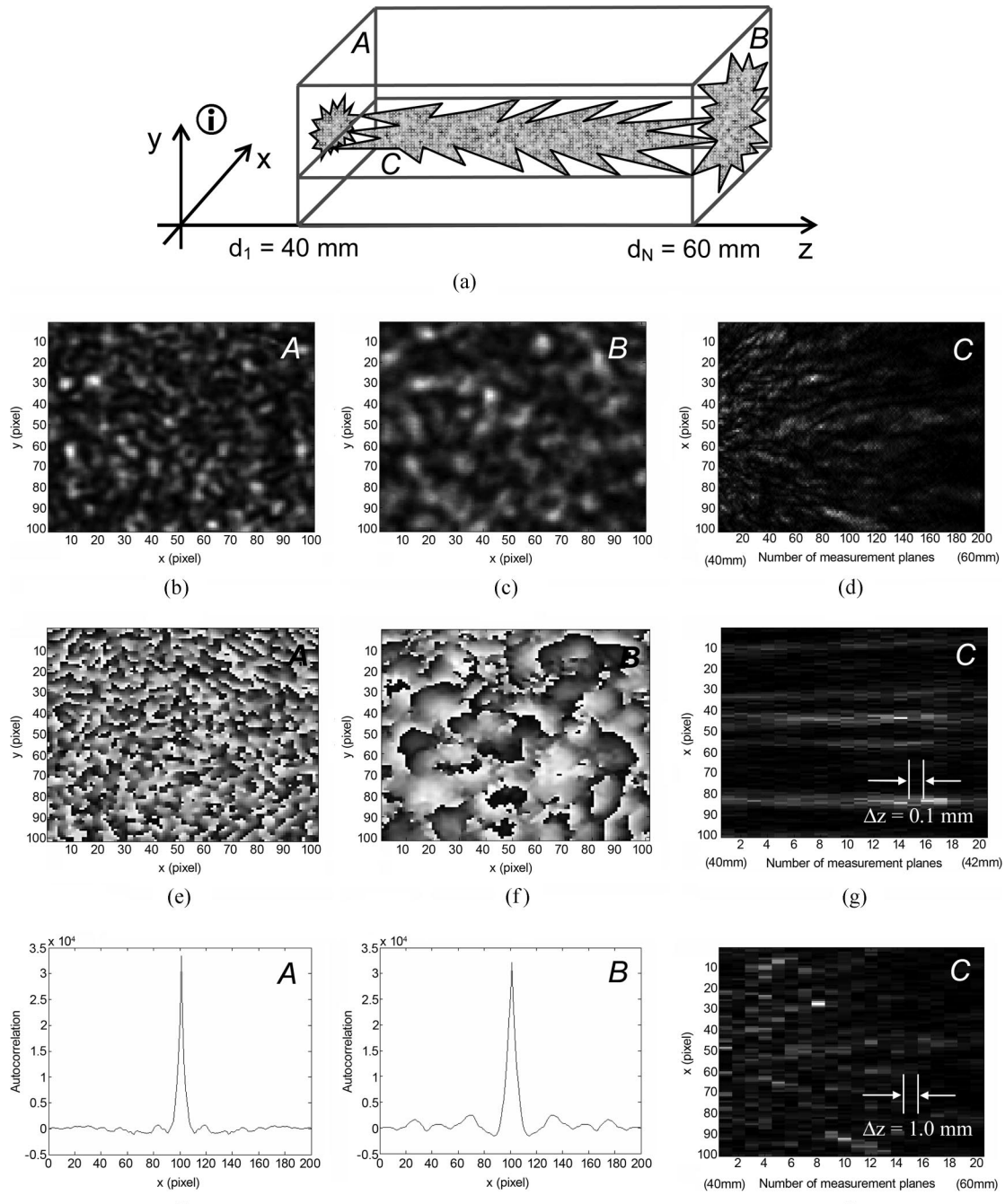

Fig. 14. (a) Diagram of volume speckle field; (b) and (c) sections of intensity measurements at transverse planes A and B, respectively; (e) and (f) the corresponding phase distributions; (h) and (i) the corresponding phase autocorrelations. (d) Section of intensity measurements in longitudinal plane C; (g) and (j) longitudinal intensity distributions from 20 measurement planes for $\Delta z = 0.1$ mm and $\Delta z = 1.0$ mm, respectively.

planes A and B, respectively. In plane A the speckle grains are relatively small with some grains visibly pixelated. The intensity saturations where merged speckle bright spots extend over a large area are observed to be minimal in this plane. In plane B the speckle grains are expectedly bigger and more enhanced and the intensity levels are still above detector sensitivity threshold. For visualization of the speckle phase distribution within the volume, the wave field reconstructed using only 20 intensity measurements at a 1 mm distance interval is investigated at different planes. Figures 14(e) and 14(f) are sections of the reconstructed wrapped phase distributions in planes A and B, respectively. Qualitatively, the observed random phase structures exhibit distinct characteristic mean size in each of these measurement planes. The mean speckle size is taken to be the distance when the phase (or intensity) auto-

correlation function (first kind Bessel function of first order) first crosses zero.[17] For thorough discussions of phase and field autocorrelations, readers are referred to Refs. 17–19. In approximating the mean speckle size the following relations for speckle coherence length (Λ) along the transverse (x or y) and longitudinal (z) axes are conventionally used[17–19]:

$$\Lambda_{\text{trans}} \cong 1.22\lambda z/D, \tag{3}$$

$$\Lambda_{\text{long}} \cong 8\lambda(z/D)^2, \tag{4}$$

where λ is the wavelength, z is the distance between the sample and the measurement planes, and D is the diameter of a uniformly illuminated circular scattering sample. Figures 14(h) and 14(i) are line scans through the centers of the 2D autocorrelation plots of the reconstructed phase shown in Figs. 14(e) and 14(f), respectively. In this experimental investigation the mean speckle size is obtained from the FWHM of the phase autocorrelation and is found to be 30.15 μm (~4.5 pixels × 6.7 μm/pixel) and 40.2 μm (~6 pixels × 6.7 μm/pixel) for transverse planes A and B, respectively. The calculated speckle sizes for planes A and B using Eq. (3) are 31 and 46 μm, respectively, in good agreement with measured results. Note that although the calculation for transverse mean speckle size is only statistical it serves as a useful guide for the object size and position from detector. In addition to speckle resolution and optimal intensity levels, the speckle field in the transverse directions must be sufficiently covered by the detector sensing area up to the last measurement plane.

Figure 14(d) shows the longitudinal speckle distribution in plane C generated from a cross section of the stack of intensity measurements. The quadratic relationship between the longitudinal mean speckle size and the distance from scatterer [Eq. (4)] accounts for why the speckles become more and more elongated along the $+z$ axis (the elongated shapes of speckles are sometimes likened to those of "cigars" or "worms"). Using Eq. (4) the approximate range of speckle size in the longitudinal direction (from 40 to 60 mm) is 1.01 to 2.28 mm. This statistical range of values serves as a useful guide for the sequential measurement distance being in the same order of magnitude. A large measurement distance means the depth of the volume speckle field will also be large. The limited detector sensing area may not be able to effectively record the volume speckle field, and the reconstruction performance of the SBMIR technique will decrease. An important comment is in order for the case when the measurement distance is very small. For such small distances the change in the intensity distributions between successive planes might not be substantial and this could also decrease the performance of the technique. For visualization and analysis of this condition the longitudinal intensity distributions are examined for varying measurement distances. Figures 14(g) and 14(j) are the longitudinal intensity distributions for distance intervals of $\Delta z = 0.1$ mm and $\Delta z = 1.0$ mm, respectively. The variation in the intensity distribution along the z axis is evidently more substantial in the case of the $\Delta z = 1.0$ mm measurement distance [Fig. 14(j)]. The variation in the longitudinal speckle intensity distribution is crucial in the reconstruction process.

The reconstruction process involves the propagation of a wave function from one plane to another with the amplitude derived from the square roots of the intensity measurements and the calculated phase, which is initially a constant. The sequential propagation of the wave function between adjacent measurement planes and iterations of the process makes changes in the wave function and gradually refines the phase. Hence the mechanism behind the reconstruction using the SBMIR technique depends not on the measured intensities *per se* but on the relationships between the sequentially measured intensities. If the change in the intensity distributions from one measurement plane to the next is not substantial, as it is in the case for the $\Delta z = 0.1$ mm measurement distance [Fig. 14(g)], the wavefront does not reconstruct appreciably. Furthermore, propagating the wave function over an increased number of intensity distributions obtained at small measurement distances will still not enhance the reconstruction. On the other hand, if the change in intensity distributions is substantial, as it is in the case for the $\Delta z = 1.0$ mm measurement distance [Fig. 14(j)], the wavefront will be reconstructed appreciably in the course of the SBMIR process.

E. Enhanced Resolution Method

To improve the sampling of the speckle intensity patterns, the enhanced resolution method was employed by recording at each plane four 1024 × 1024 pixel images and combining them into one 2048 × 2048 pixel super image. Each of the 1024 × 1024 images is obtained by shifting the camera a distance of a half-pixel (3.35 μm) in the horizontal and vertical directions (the additional motorized precision stages are not shown in Fig. 1). The test object used is a transmission mask with a ground glass diffuser. The width of the object is 3 mm with a thickness of ~250 μm. Figures 15(a) and 15(b) show zoomed-in images of two speckle grains digitized into matrices of square camera pixels corresponding to the original resolution and doubled resolution of the detection system, respectively. Figure 15(c) shows a sample reconstruction from a set of 1024 × 1024 pixel images. Notice some distortions especially in the leftmost element letter "B." Figure 15(d) shows reconstruction from a set of 2048 × 2048 pixel subpixel scanned super images where the same element letter B has a much better image quality. Evidently the enhanced resolution method improves the sampling of speckle patterns and results in better quality reconstructions. Since the ability of the detection system to resolve finer speckles is increased, the stringent re-

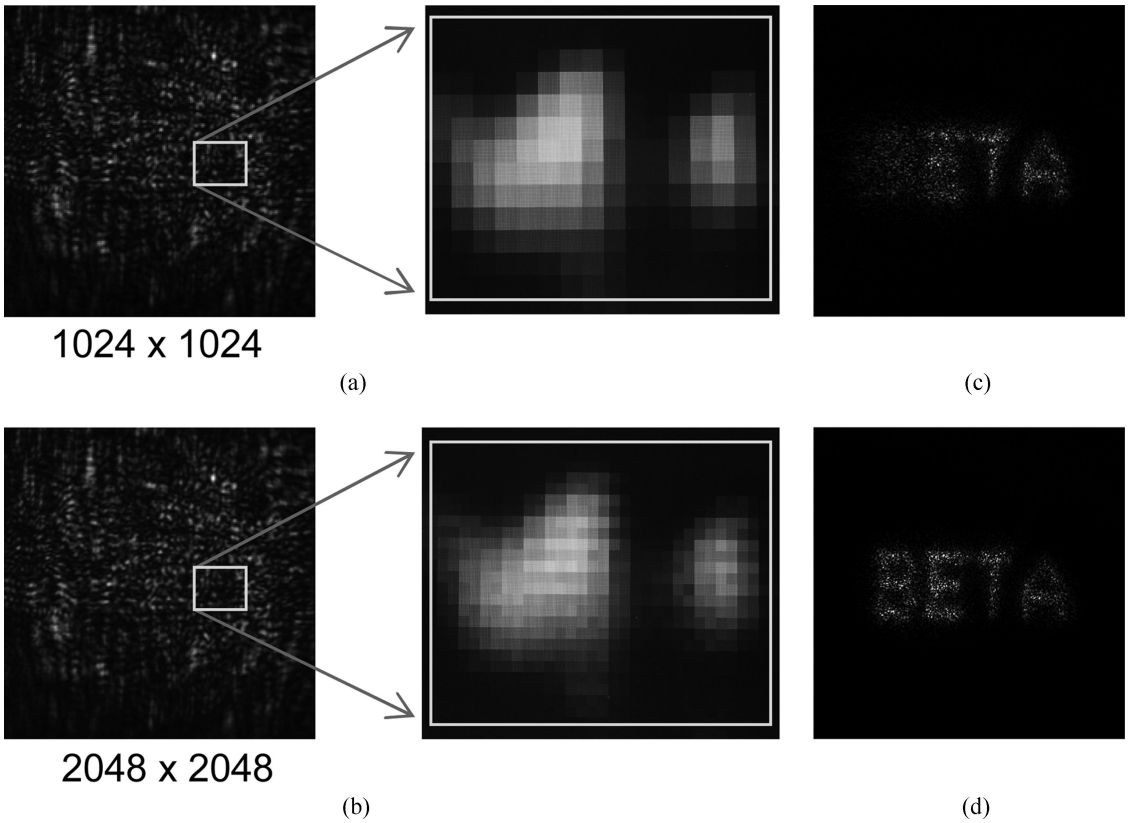

Fig. 15. Reconstructions using the enhanced resolution method. (a) Zoomed-in image from a 1024 × 1024 pixel intensity measurement. (b) Zoomed-in image from a 2048 × 2048 pixel super image intensity measurement. (c) Reconstruction from a set of 1024 × 1024 pixel intensity measurements. (d) Reconstruction from a set of 2048 × 2048 pixel super image intensity measurements.

quirement on the size of the object imposed by the sampling condition may effectively be reduced.

5. Conclusions

We have demonstrated the reconstructions of wavefronts from diffusely transmitting and reflecting objects using the SBMIR technique. The effects of different parameters on the quality of reconstructions were investigated and the results can be summarized in the following: (1) Quality of reconstructions increases with an increasing number of intensity measurements and iterations. Based on the correlations of the reconstructions in the simulations and supported by experimental results, 20 intensity measurements and two iterations may be sufficient for satisfactory wavefront reconstruction. (2) Quality of reconstructions improves significantly within some range of minimum measurement distance. For the particular objects used, a measurement distance of $\Delta z = 0.5$ mm may be set to achieve satisfactory wavefront reconstruction. The qualities of transverse and longitudinal speckle intensity distributions that result in wavefront reconstruction using the SBMIR technique are characterized. The transverse intensity distributions within the speckle volume must exhibit enhanced resolution and optimal intensity levels and must be sufficiently covered by the detector sensing area. The longitudinal intensity distribution must demonstrate variations within the sequential measurement distance. An enhanced resolution method improved the recording of speckle patterns and this, in turn, resulted in better quality reconstructions. The improved sampling, especially of the smaller size speckles, allows the possibility of applying the SBMIR technique to larger extended objects.

The authors gratefully acknowledge the support of the German Research Foundation (DFG) under grant 05111/19-1. P. Almoro thanks the University of the Philippines for a postdoctoral fellowship. The authors thank Fucai Zhang and Roger Groves for valuable assistance with the instrumentation for this research.

References

1. L. Yaroslavsky, *Digital Holography and Digital Image Processing: Principles, Methods, Algorithms* (Kluwer, 2004).
2. P. K. Rastogi, *Digital Speckle Pattern Interferometry and Related Techniques* (Wiley, 2001).
3. A. Barty, K. A. Nugent, D. Paganin, and A. Roberts, "Quantitative optical phase microscopy," Opt. Lett. **23,** 817–819 (1998).
4. J. Wu, U. Weierstall, and J. C. H. Spence, "Diffractive electron imaging of nanoparticles on a substrate," Nat. Mater. **4,** 912–916 (2005).
5. R. W. Gerchberg and W. O. Saxton, "A practical algorithm for the determination of phase from image and diffraction plane pictures," Optik (Stuttgart) **35,** 237–246 (1972).
6. G. Yang, B. Dong, B. Gu, J. Zhuang, and O. K. Ersoy, "Gerchberg–Saxton and Yang–Gu algorithms for phase re-

trieval in a nonunitary transform system: a comparison," Appl. Opt. **33,** 209–218 (1994).
7. J. R. Fienup, "Phase retrieval algorithms: a comparison," Appl. Opt. **21,** 2758–2769 (1982).
8. M. R. Teague, "Deterministic phase retrieval: a Green's function solution," J. Opt. Soc. Am. **73,** 1434–1441 (1983).
9. C. J. R. Sheppard, "Three-dimensional phase imaging with the intensity transport equation," Appl. Opt. **41,** 5951–5955 (2002).
10. E. Kolenović, "Correlation between intensity and phase in monochromatic light," J. Opt. Soc. Am. A **22,** 899–906 (2005).
11. G. Liu and P. D. Scott, "Phase retrieval and twin-image elimination for in-line Fresnel holograms," J. Opt. Soc. Am. A **4,** 159–165 (1987).
12. Y. Zhang, G. Pedrini, W. Osten, and H. Tiziani, "Whole optical wave field reconstruction from double or multi in-line holograms by phase retrieval algorithm," Opt. Express **11,** 3234–3241 (2003).
13. Y. Zhang, G. Pedrini, W. Osten, and H. Tiziani, "Image reconstruction for in-line holography with Yang–Gu algorithm," Appl. Opt. **42,** 6452–6457 (2003).
14. G. Pedrini, W. Osten, and Y. Zhang, "Wave-front reconstruction from a sequence of interferograms recorded at different planes," Opt. Lett. **30,** 833–835 (2005).
15. J. Kornis and B. Gombkötő, "Application of super image methods in digital holography," in *Optical Measurement Systems for Industrial Inspection IV,* W. Osten, C. Gorecki, and E. L. Novak, eds., Proc. SPIE **5856,** 245–253 (2005).
16. J. W. Goodman, *Introduction to Fourier Optics,* 2nd ed. (McGraw-Hill, 1996).
17. I. Freund and D. A. Kessler, "Phase autocorrelation of random wave fields," Opt. Commun. **124,** 321–332 (1996).
18. Q. B. Li and F. P. Chiang, "Three-dimensional dimension of laser speckle," Appl. Opt. **31,** 6287–6291 (1992).
19. J. W. Goodman, *Statistical Optics* (Wiley, 1985).